Separation and Purification Technology 233 (2020) 116061

Contents lists available at ScienceDirect

Separation and Purification Technology

journal homepage: www.elsevier.com/locate/seppur

Selective permeation of L-tyrosine through functionalized single-walled carbon nanotube thin film nanocomposite membrane

Monti Gogoi[a,b], Rajiv Goswami[a,b], P.G. Ingole[a], Swapnali Hazarika[a,b,*]

[a] Chemical Engineering Group, Engineering Science & Technology Division, CSIR-North East Institute of Science and Technology, Jorhat 785006, Assam, India
[b] Academy of Scientific and Innovative Research, CSIR-NEIST Campus, India

ARTICLE INFO

Keywords:
Functionalized carbon nanotubes
Racemic resolution
Enantiomeric excess
Enantioseparation

ABSTRACT

In the present work, we demonstrated a strategy to render an enantioselective nature to otherwise hydrophobic Single-walled carbon nanotubes (SWCNTs) via a simple covalent functionalization. The covalent functionalization was initiated on the SWCNTs surface by incorporating a −COOH group followed by chlorination of the carboxylic group into acid chlorides and terminated with an amidation reaction using D-tryptophan as the chiral probe. Subsequently, the functionalized SWCNTs were assembled into a thin film nanocomposite membrane following a phase inversion method. Finally, the enantioselectivity of the developed membrane was tested by treating a racemic mixture of tyrosine on the membrane, where the D-isomer was preferentially adsorbed on the membrane while the L-isomer was selectively allowed to transport through it. In order to optimize the permselective properties of the membrane, different process parameters such as mass loading of SWCNTs, concentration of feed, applied pressure and reaction temperature were varied in a pressure-driven membrane process and highest enantiomeric excess up to 98.86% was obtained under optimized conditions which include the concentration of FSWCNTs as 0.2% in the membrane, operation pressure of 4 bar, feed concentration less than 0.1 mmol·L^{-1} and operation temperature of 35 °C. Moreover, the effect of concentration of FSWCNT in the dope solution was also examined to increase the thermal as well as mechanical properties and antifouling behavior of the membrane.

1. Introduction

Chiral compounds are very much essential for biological systems and the effect of enantiomers may vary due to the stereoselective nature of the reactions inside the body. Homochiral compounds react with individual racemic drug separately and stabilize specific isomer by a different throughway to give a separate pharmacological output [1,2]. Thus, a particular isomer has a definite medicinal exertion and other isomer is in active or has toxic effects [3,4]. L-tyrosine is widely used amino acid for the production of neurotransmitters; derivative crop out to be anti-stress for acute stressors and may retain stress-induced memory loss [5]. Therefore, development of an adequate resolution process for separation of isomers of racemic tyrosine has gained a lot of attention.

Various methods like adsorption process, chromatographic methods, diastereomeric crystallization etc. have been used for the segregation of single isomer from its racemic blend [6]. However, in these methods resolving molecules and hosts cannot be retrieved easily and prudently. Separation of one isomer from a racemic mixture via membrane is effective as it is a continuous process handling large amount of target molecules. In addition to this, membrane-based methods are cost-effective and environment friendly [7,8]. These processes can be easily pecked up hence exquisitely looked over in the current scenario. Optical resolution process involves a membrane which performs as a choosy obstruction and it permeates the desiderate molecule. Apparently, the membrane should acquire a chiral identification mechanism which eventually acts as a central dogma that will distinguish the isomers from racemic mixtures [9,10]. Moreover, permeation is thought-about as a propitious technology for the segregation of amino acids in the form of racemic mixture [11].

As the separation of the racemic mixtures turns out to be a difficult aspect, researchers have adopted various methods to develop specific membranes by introducing chiral moiety into the polymeric membranes [11,12], preparing chiral ligand exchange membranes [13], development of quint essential enantioselective composite membrane [14], amphiphilic polymer conetworks as membrane [15], etc. for chiral

* Corresponding author at: Chemical Engineering Group, Engineering Science & Technology Division, CSIR-North East Institute of Science and Technology, Jorhat 785006, Assam, India.
E-mail address: shrrljt@yahoo.com (S. Hazarika).

https://doi.org/10.1016/j.seppur.2019.116061
Received 15 May 2019; Received in revised form 6 August 2019; Accepted 10 September 2019
Available online 10 September 2019
1383-5866/

separation. Among these, modifying the polymeric matrices with definite molecular identification ability greatly leads to the development of novel membranes with proper selectivity for efficient separation of chiral mixtures [16,17]. Moreover, they possess several limitations such as poor mechanical strength, low flux due to their cross-linking degree, lower separation efficiency and recognition ability, etc. Hence there is a great demand in the development of novel membranes through innovative design in order to meet the shortcomings of the previously developed platforms and also to fulfill the needs of the modern science and technology.

Carbon nanotubes (CNTs) can be used in various applications such as extraction of drugs and pollutants, enantiomeric separation of drugs [18]. But due to the hydrophobic nature, high enantioselection cannot be obtained if CNTs are used in pure form. In order to avoid this issue, CNT's are to be functionalized for effective applications [19,20]. However, development of functionalized CNT's for membrane application in enantiomer separation is limited. Due to the hydrophobic nature of the pristine CNTs, high enantioselection cannot be obtained. Chiral functionalization of CNT's makes it possible to interact with chiral compounds and separate the enantiomer [21]. In the field of chiral and achiral separation, the functionalized CNTs have become an upcoming topic of study. The process of functionalization of CNTs can be easily done which efficiently and rapidly intensifies the separation selectivity thereby enhancing the chiral separation process [22,23].

Due to the hydrophobic nature of the surface, immaculate CNTs do not dissolve in aqueous solutions. Functionalization of CNT not only results in enhancement of biocompatibility of the technique but also mitigate the additional use of stabilizing agent. In view of the importance of both functionalized CNTs and the membrane, the present work demonstrates the functionalization of SWCNT which incorporate the D-tryptophan as the chiral selector. Previously reported literature on enantiomeric separation with the aid of CNTs basically based on chromatographic separation method, but the current work deals with the utilization of CNTs in the form of a membrane which provides an opportunity to enantioseparation of chiral molecules in large scale. Moreover use of FSWCNTs was found to be beneficial for improving the antifouling behavior of the membrane which in turn kept a high flux of L-tryosine for longer time duration. The membrane is also thermally and mechanically very stable unlike polymeric membrane and shows high magnitude of enantiomeric excess (upto 98.86%) towards separation of racemic mixture of tyrosine. Looking at the emerging potential of SWCNTs membrane for practical use in industrial scale, the present work indicates that the FSWCNTs membrane could be an ideal platform for enantioseparation in pharmaceutical industry.

2. Materials and methods

2.1. Materials

Single walled carbon nanotubes, SWCNT (Assay: min.90%, OD: 1–2 nm, Length: 5–30 μm) was procured from M/s Sisco Research Laboratory Pvt. Ltd., Mumbai, India. Polysulfone (average molecular weight 30,000) was obtained from M/s SIGMA-Aldrich Chemical Company, USA. Thionyl Chloride was obtained from M/s Merck Specialities Private Limited, Mumbai, India. Ethanol, Dimethyl formamide, Nitric acid, Sulphuric acid, Methanol and N-methyl pyrrolidine (NMP) was supplied from M/s RANKEM range of laboratory chemicals, Gujarat, India. Polyethylene Glycol (PEG) was procured from M/s Sisco Research Laboratory Pvt. Ltd (SRL), India. DL-, D-, L-tyrosine and D-tryptophan (> 98%) was obtained from M/s TCI Chemicals (India) Pvt. Ltd.

2.2. Method

2.2.1. Functionalization of SWCNTs

Prior to the carboxylation step, the pure CNTs were continuously sonicated in a proportion of 15 mg SWCNT in 500 mL ethanol for 45 min in order to segregate the clusters of CNTs. This pretreatment eventually improves their individual interaction in the acid treatment step thereby making them more reactive. Then, they were filtered through a Poly Tetra Fluoro Ethylene (PTFE) membrane of pore size 0.2 μm using a vacuum pump. Eventually, the derived SWCNTs were dehydrated overnight in a vacuum oven at 100 °C.

5 mg of pretreated SWCNT was immersed in a solution of 6.5 mL of HNO_3/H_2SO_4 of ratio 1:3 (v/v) and sonicated the mixture at 30 °C for a period of 6 h. After this step, the dispersed SWCNT was filtered through a 0.2 μm PTFE membrane. The acid treated SWCNTs were continuously washed with distilled water and its pH was measured after every wash. The washing process continued until the pH of the filtrate was 7. Further the product was dried overnight in a vacuum oven at 120 °C.

5% of SWCNT-COOH was treated with a mixture of 12:1 (v/v) of thionyl chloride and Dimethyl formamide (DMF) under reflux condition at a temperature of 60 °C for 52 h. The mixture was than cooled to room temperature and rinsed with 10 mL of 1:1 (v/v) of THF and ethanol solution, filtered and desiccated overnight.

15 g of D-tryptophan was added to a mixture of 75:25 (v/v) ethanol and water. An approximate amount of 5% of SWCNT-COCl was introduced to the above solution under reflux condition at a temperature of 80 °C upon consistent stirring for 8 h. The residue was segregated by filtration method, dried at 60 °C and was further washed with a solution of water and ethanol in order to remove excess residual tryptophan moieties. Finally, the functionalized SWCNTs (FSWCNTs) were completely dried in a vacuum oven at 70 °C.

In order to quantify the amount of D-tryptophan attached to the FSWCNTs, defunctionalization of FSWCNTs was done via hydrolysis in homogeneous THF solutions with NaH. This led to the formation of dark-colored precipitates which was further characterized by various spectroscopic techniques.

2.2.2. Preparation of membrane

Flat sheet membranes were prepared from a homogeneous mixture of 18.22% of Polysulfone (PSf), 0.15% of Polyethylene glycol (PEG-1500) as the additive and 81.62% of NMP as the solvent. To the homogeneous solutions different concentration of FSWCNTs (0.025%, 0.05%, 0.1% and 0.2%, w/v) was separately added in order to generate the dispersed nanocomposite casting solutions. The weight % of FSWCNTs was initially selected arbitrarily and gradually the concentration was varied. The solutions were continuously stirred for 6 h at a constant temperature of 35 °C. The membranes were cast on a clean glass plate with a casting Knife. The membranes were dipped in water and kept overnight to remove the solvent. Membranes were dried at ambient conditions and finally characterized by spectroscopic methods.

2.2.3. Analytical techniques

FSWCNTs were analyzed by Fourier Transform Infrared Spectroscopy (FTIR), Field-emission scanning electron microscopy (FESEM), Raman and X-ray Photoelectron Spectroscopy (XPS). Nanocomposite membranes were characterized by FTIR, XPS, Thermogravimetric Analysis (TGA), Atomic Force Microscopy (AFM), FESEM, HRTEM, Electrokinetic Analyzer and contact angle analysis. The FTIR spectra were recorded with Perkin Elmer, 2000 Infrared spectrophotometer which helps to determine the functional groups on the surface of CNT by measuring the stretching frequencies. Raman Spectroscopy was done using the Laser Micro Raman System, Horiba Jobin Vyon, Model LabRam HR wherein the energy of the generated scattered photons determined the vibrational modes of the sample. TGA was determined using a Perkin Elmer PC series, DSC 7 under nitrogen atmosphere at a heating rate of 10 °C. This is found to be an effective technique for the study of decomposition kinetics and perceptible experimentation of the prepared composite membranes as a function of annealing temperature. The surface morphology of the membranes was studied using AFM (AFM, Nanomagnetics: hpAFM), Field-emission

scanning electron microscopy (FESEM, LEO 1427 VP, UK) and High-Resolution Transmission Electron microscopy (HRTEM, JEOL, Japan, JEM 2100). Both these techniques affirmed the surface and structural changes of FSWCNTs. The surface charge and its changes are described by Zeta potential (ζ) which is determined by SurPASS™ Electrokinetic Analyzer (Anton Paar, Austria). The Zeta potential is determined from streaming potential and current measurement which is measured from Helmholtz-Smoluchowski Equations. The contact angle of the membrane was determined by the contact angle meter (DM-501, Kyonea Interface Science) at 25 °C. The probe liquid used in this measurement was water. The elements present in the FSWCNT and nanocomposite membranes were resolved from an X-ray photoelectron spectrophotometer, Thermo Fisher Scientific: ESCALAB Xi$^+$. The concentration of permeate was determined by a UHPLC model Dionex (Thermo Fisher Co.) using CHIROBIOTIC ® T (25 cm × 4.6 mm, 5 µm) chiral column at wavelength 200 nm. The mobile phase used was 0.02% of aq. HCOOH and methanol (50:50) with a flow rate of 0.5 mL min^{-1}.

2.2.4. Separation study

Separation experiments were performed in a series of three different two-compartment membrane cell applying stirring speed 200 rpm in the feed tank and at a definite pressure and temperature. The volume of the cell in the feed portion and permeate portion was 300 mL and 150 mL respectively. The membrane of area 19.20 cm^2 was lodged between the compartments and connected to the stock solution of 1000 mL. Aqueous solutions of DL-tyrosine (pH 4.8) was stirred continuously for 8 h and gyrated by peristaltic pump. Experiments were conducted by varying the pressure, temperature and concentration. During the permeation period, samples were collected from the permeate side at a gradual interval of 1 h and analyzed by UHPLC. For a continuous experimental set up, the permeation flux and the enantiomeric excess value was calculated based on the equations mentioned in our previous work [11]. The flow diagram of the permeation set-up is given in Fig. 1.

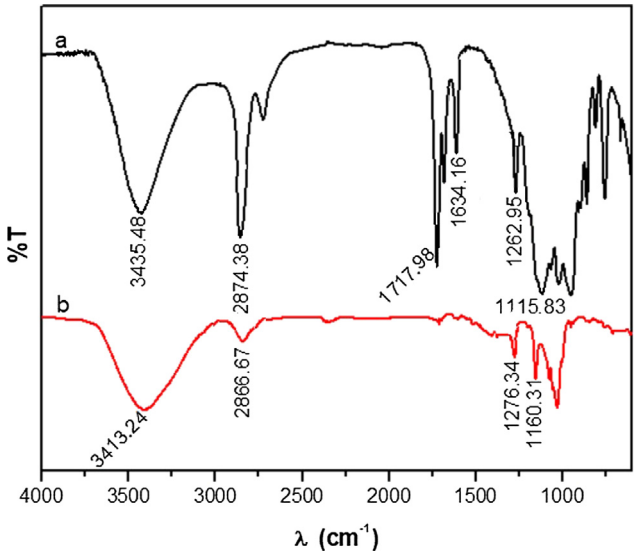

Fig. 2. FTIR spectra of (a) FSWCNTs based nanocomposite membrane, M_4 and (b) Pure Polysulfone membrane.

3. Results and discussion

3.1. Characterization of the FSWCNTs based nanocomposite membranes

Fig. 2 depicts the FTIR spectra of FSWCNTs based nanocomposite membrane, M_4 containing 0.2% of concentration of FSWCNTs wherein the spectra of Pure Polysulfone (PSf) membrane is also shown for comparison. The characteristic peaks at 1262.95 cm^{-1}, 1717.98 cm^{-1} and 2874.38 cm^{-1} in Fig. 2(a) are attributed to C—O—C, —COOH and $-CH_3$ group. Similarly, in Fig. 1(b) peaks at 1276.34 cm^{-1} and 2866.67 cm^{-1} corresponds to C—O—C and $-CH_3$ group present in PSf membrane. The broad peak at 3413.24 cm^{-1} in Fig. 2(b) corresponds to the O—H stretching which arises due to the absorption of water during analysis. Additional peaks were observed in case of FSWCNTs based

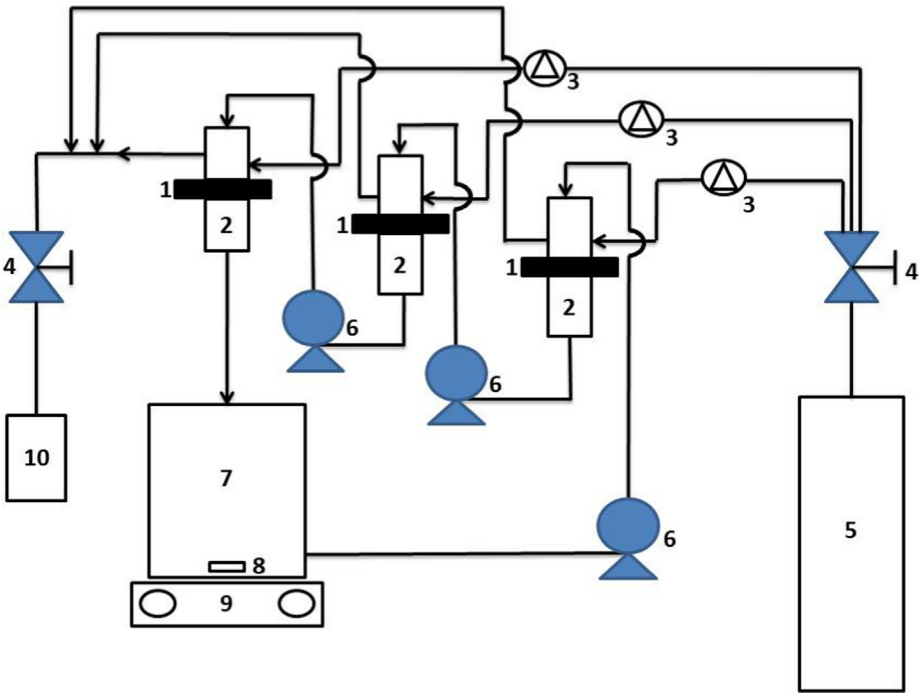

Fig. 1. Flow diagram of permeation set-up (1) Nanocomposite membrane, (2) Two compartment membrane cell, (3) Pressure gauze, (4) Valve, (5) Nitrogen cylinder, (6) Peristaltic pump, (7) Feed tank, (8) Magnetic needle, (9) Magnetic stirrer, and (10) Gas outlet.

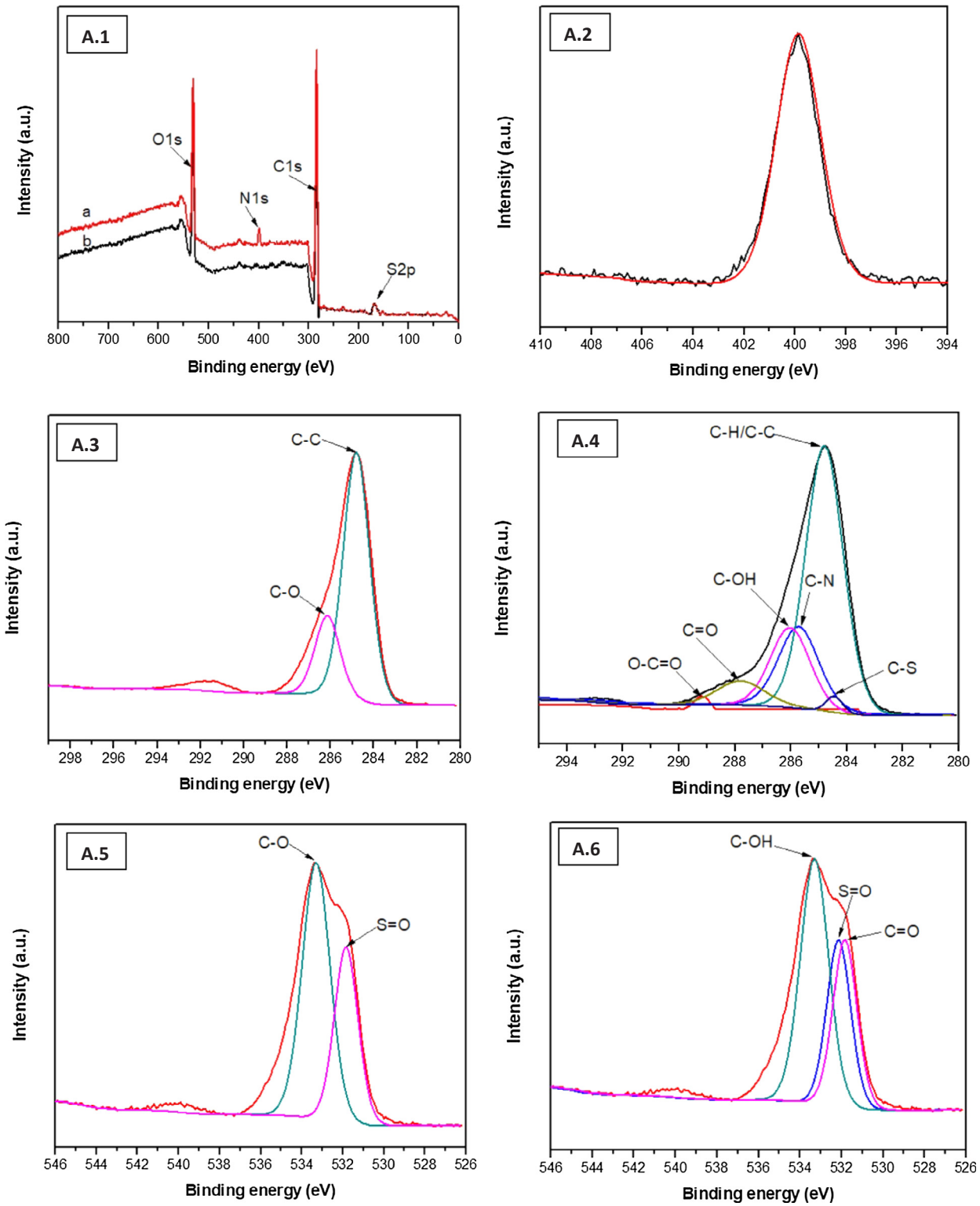

Fig. 3. XPS spectra (A.1) survey scan of (a) FSWCNTs based nanocomposite membrane (b) PSf membrane; (A.2) N1s nano scan, (A.4) C1s nano scan, (A.6) O1s nano scan, (A.8) S2p nano scan of FSWCNTs based nanocomposite membrane; (A.3) C1s nano scan, (A.5) O1s nano scan, and (A.7) S2p nano scan of PSf membrane.

nanocomposite membrane. It was observed that the absorption band at 3435.48 cm^{-1}, 1634.16 cm^{-1} is attributed to the NH stretching vibration originating from the D-tryptophan attached to the FSWCNTs which is somewhat absent in the PSf membrane. The peak at 1013.19 cm^{-1} ascribes to the C—N vibrations. The characteristic peaks at 1115.83 cm^{-1} in Fig. 2(a) and 1160.31 cm^{-1} in Fig. 1(b) corresponds to the stretching of C—SO_2—C bonds present in the Polysulfone [6,24]. From the IR analysis it is seen that the FSWCNTs are well dispersed in the PSf membrane.

XPS characterization was used to evaluate the degree of amine functionalization in FSWCNTs based membrane. The elemental surface composition of the pure Polysulfone (PSf) and FSWCNTs based nanocomposite membrane; M_4 was examined by this technique as shown in Fig. 3. From the survey spectra (A.1), the elements detected for the

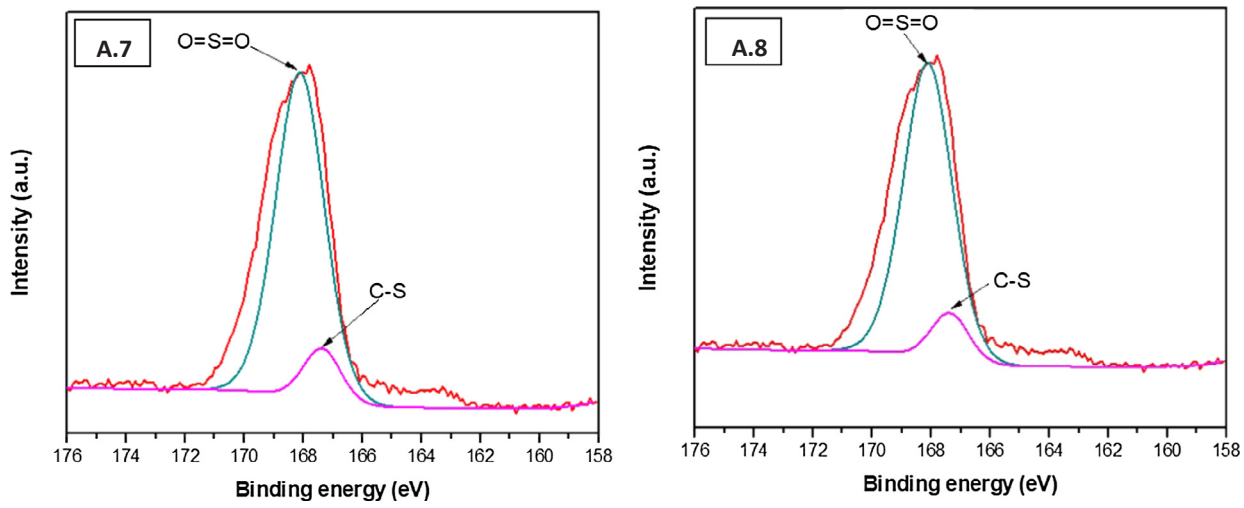

Fig. 3. (*continued*)

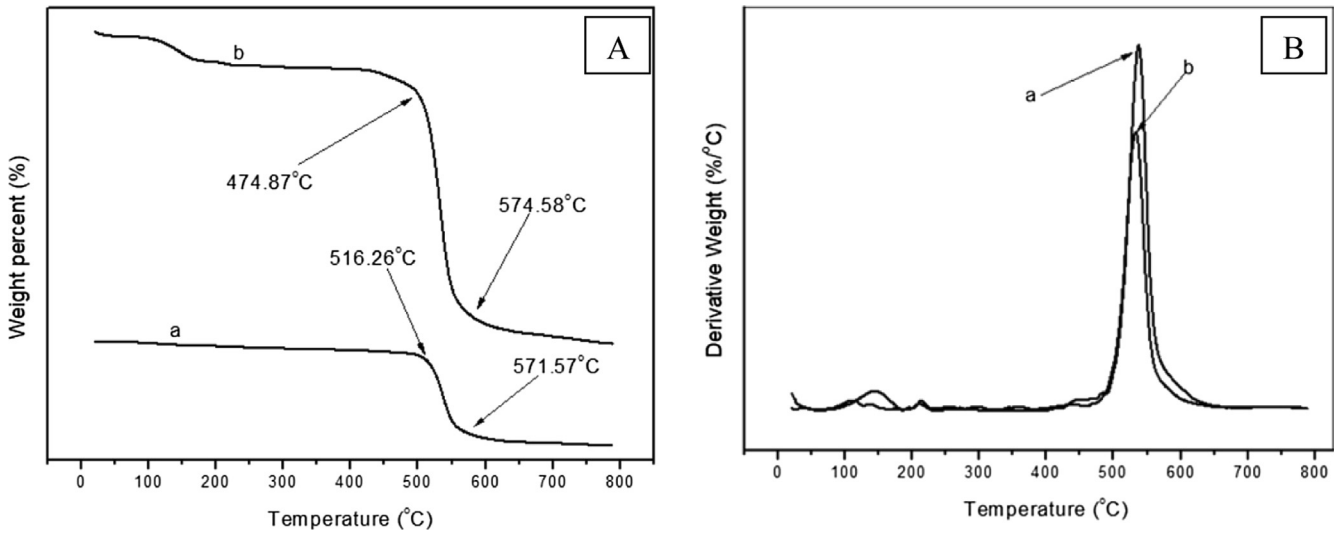

Fig. 4. (A) TGA (B) DTG spectra of (a) FSWCNTs based nanocomposite membrane, M4 and (b) Pure Polysulfone membrane.

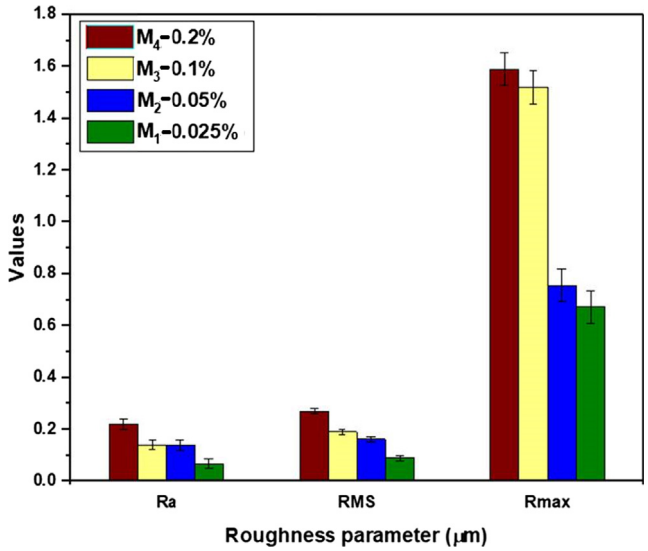

Fig. 5. Roughness parameters of the FSWCNTs based nanocomposite membranes.

nanocomposite membranes were C, O, N and S whereas for PSf membrane, only elements detected were C, O and S. For both PSf and nanocomposite membrane, the S2p, C1s, and O1s spectrum peaks were observed at 167.3, 286 eV and 531.7 eV respectively. An additional peak was observed in the spectra of the nanocomposite membrane at 399.6 eV which corresponds to N1s which was further confirmed from the nano scan as shown in Fig. 3(A.2). The O/C ratios of the PSf and nanocomposite membrane are 0.19 and 0.26 respectively. This increase is due to the introduction of more oxygen from the FSWCNTs in the M_4 membrane. The C1s nano scan for PSf membrane revealed two different peaks at a binding energy of 284.5 eV and 286 eV attributing to C—C and C—O respectively whereas for the M_4 membrane, six different peaks were observed at a binding energy shift of 284.5 eV, 285.2 eV, 285.7 eV, 285.9 eV, 287.8 eV and 289.2 eV corresponding to C—C, C—S, C—N, C—OH, C═O and O—C═O respectively. This confirms the successful functionalization of SWCNTs. Further for O1s nano scan, two peaks were obtained at a binding energy shift of 532.1 eV and 533.5 eV which is attributed to S═O and C—O present in both the membranes, Fig. 3(A.3, A.4). An additional peak was obtained for C═O at a binding energy shift of 531.5 eV for the M_4 membrane, Fig. 3(A.4). The S2p nano scan depicted two different peaks for both the membranes at a binding energy shift of 168.6 eV and 169.9 eV which corresponds to C—S and O═S═O due to the presence of polysulfone in the membrane matrix [6,25]. The notable difference in the content between PSf and

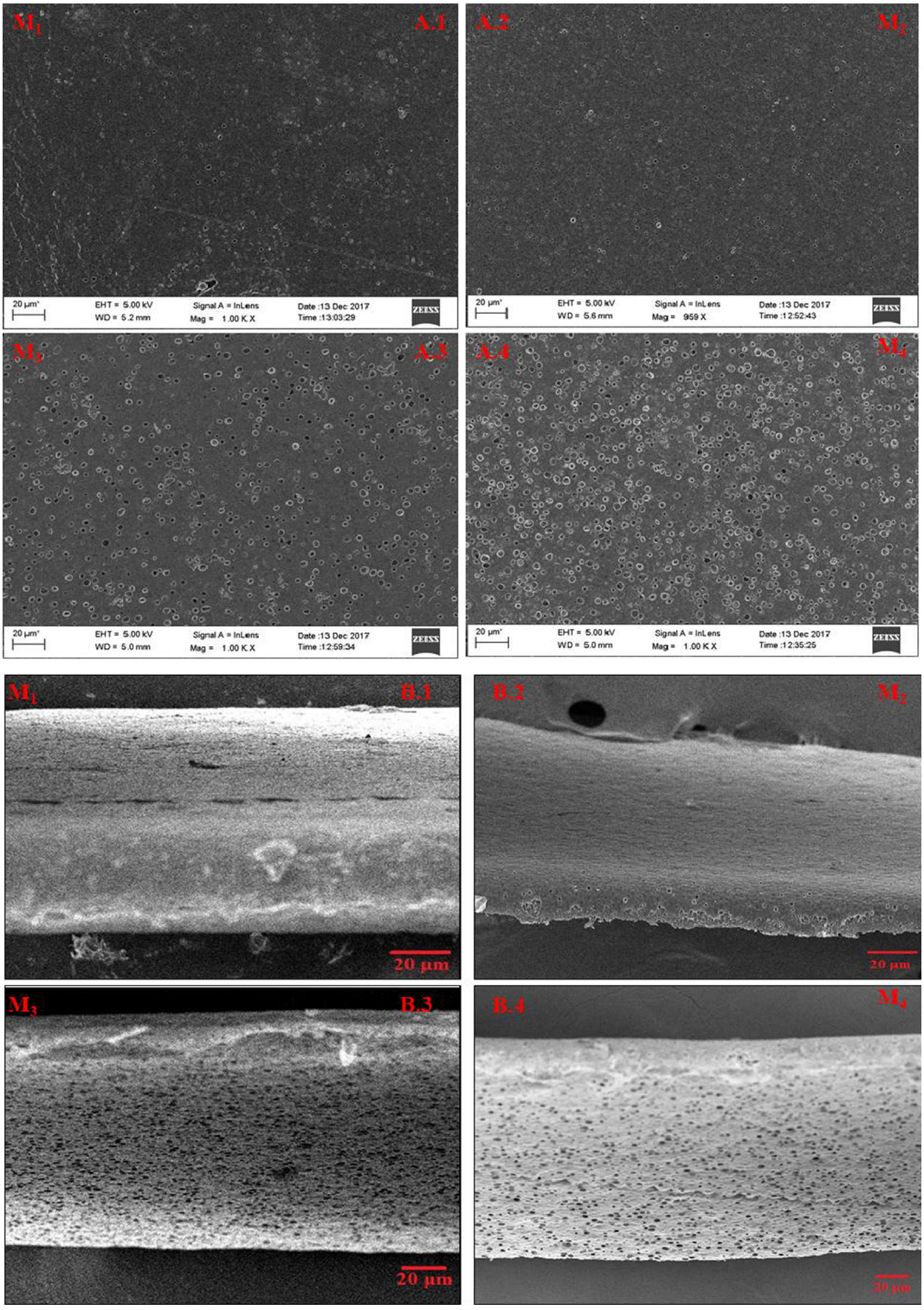

Fig. 6. FESEM images of FSWCNT nanocomposite membranes, A.1–A.4: Front view and B.1–B.4: Cross-sectional view.

M_4 membranes is likely a consequence of the step-wise functionalization done for SWCNTs.

The stability of the membrane against thermal stress was determined from the thermo gravimetric analysis which was performed under nitrogen atmosphere at a heating rate of 10 °C min^{-1}. The decomposition curves of the PSf and FSWCNTs based nanocomposite membrane M_4 are shown in Fig. 4(A). The derivative curves are also shown in Fig. S5(B). For PSf membrane, small weight loss (about 4.5 wt %) in the range of 60 °C to 120 °C was observed due to evaporation of water in the membrane surface. Both the membranes undergo two step decompositions. For PSf and M_4 membrane, decomposition occurs at 474.87 °C and 574.58 °C; and 516.26 °C and 571.57 °C respectively. Thus, it is seen that M_4 membrane containing 0.2% of FSWCNTs are thermally stable up to the temperature 516 °C. DSC analyses of the membranes were performed at a heating rate of 10 °C·min^{-1} under nitrogen atmosphere. Melting endothermic peaks obtained at different temperatures for both the membranes were shown in Fig. 4(B). The change in glass transition temperature, Tg for composite membranes

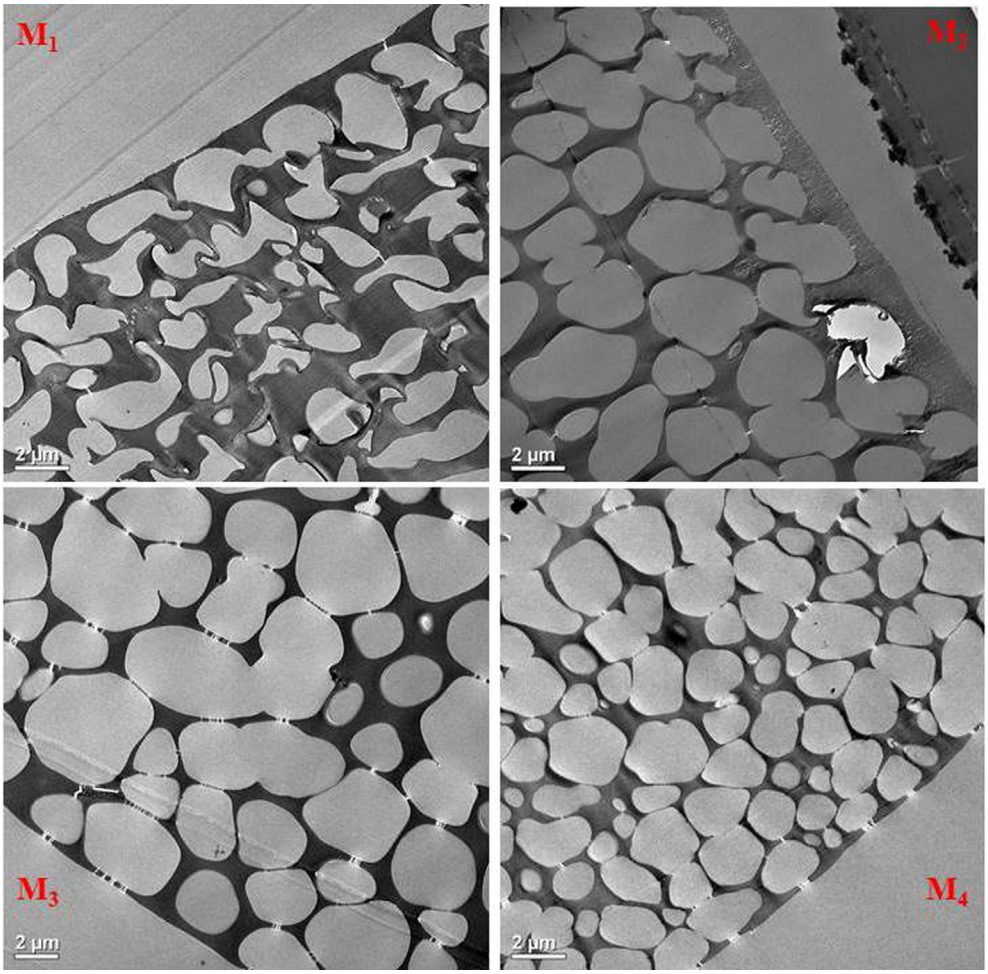

Fig. 7. HRTEM images of FSWCNT nanocomposite membranes M_1, M_2, M_3 and M_4.

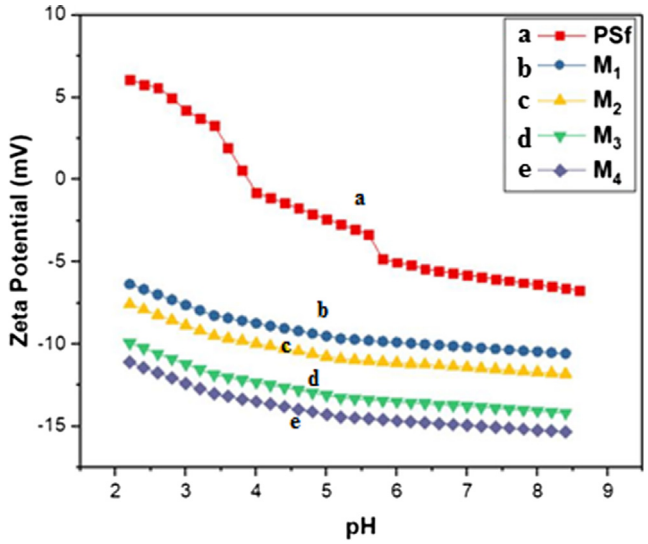

Fig. 8. pH versus Zeta potential representation of PSf and FSWCNT based nanocomposite membranes.

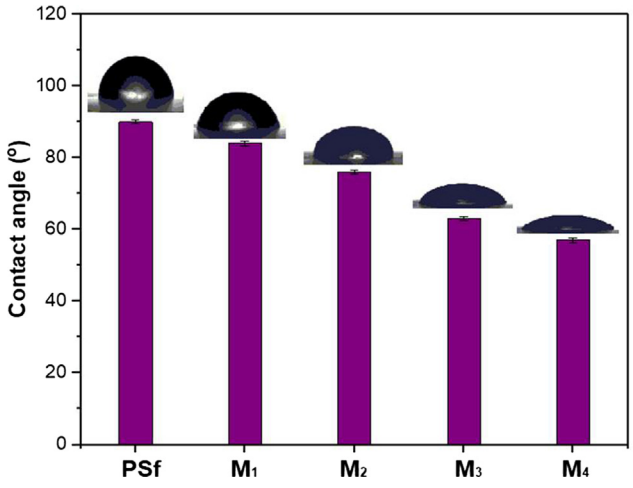

Fig. 9. Values of Water contact angle of PSf and FSWCNTs nanocomposite membranes.

were strongly influenced by the membrane pore structure because of glass transition temperature which took place on cooling due to the presence of domains of slow dynamics by thermally induced density fluctuations.

The exterior face of membranes was determined by AFM characterization, as given in the supporting information (Fig. S5). Fig. 5 below depicts the analysis of surface roughness of FSWCNTs based nanocomposite membranes M_1, M_2, M_3 and M_4 containing FSWCNT 0.025%, 0.05%, 0.1% and 0.2% respectively. Roughness parameters, including average roughness (R_a), root-mean-square of roughness (RMS) and maximum roughness (R_p) were measured in the tapping mode. It was observed that the value of root-mean-square (RMS)

Table 1
Tensile strength and contact angle of PSf and FSWCNTs based nanocomposite membranes.

Membrane	Weight % of FSWCNT	Tensile strength, σ (MPa)	Contact angle (°)
Polysulfone	0	12 ± 0.2	90 ± 2
M_1	0.025	15 ± 0.3	84 ± 2
M_2	0.05	18 ± 0.5	76 ± 2
M_3	0.1	21 ± 0.2	63 ± 3
M_4	0.2	29 ± 0.4	57 ± 2

roughness of the membrane containing higher amount of FSWCNTs is 0.27 µm which is larger than that of the membrane containing lower amount of FSWCNTs which is 0.067 µm. Thus, it indicates that the inclusion of FSWCNTs can unusually improve the roughness of membrane. With the increment in the roughness of membrane, the effective area for mass transfer increases which thereby increase the mass transfer flux.

The pictorial view of the FESEM analysis illustrates that the surface morphology and cross-sectional view of the prepared membranes (M_1, M_2, M_3 and M_4) are enhanced by the addition of FSWCNTs. Fig. 6(A.1–A.4) represents the surface images of membranes. The Fig. also reveals the fact that there occurs no agglomeration of FSWCNTs in the surface of prepared membrane. Fig. 6(B.1–B.4) gives the cross-sectional view of the FSWCNTs based nanocomposite membranes. From this Fig., it is seen that for M_4 membrane pores are uniformly distributed which are circular in shape. This uniform distribution of pores in the top surface and cross-sectional areas indicated the smooth and homogeneous morphology of the membranes.

HRTEM analysis gives an effective image which helps to analyze the internal structure of the prepared polymeric membrane because of its high resolution. It is suitable enough to visualize the surface of the membrane bearing different chemical structure. A properly mixed polymeric solutions containing concentration of FSWCNTs as 0.025%, 0.05%, 0.1% and 0.2% (M_1, M_2, M_3 and M_4) respectively was hardened by cooling to sub-zero temperature of −80 °C. It was than immersed in a 2% solution of uranyl nitrate for about 10 min and further dried in a vacuum oven at 25 °C for 2 h. A definite section (< 70 nm thick) of the stained polymeric sample was cut using a diamond knife with the help of an ultra microtome and then placed in Copper (Cu) grids. The grids were placed in desiccators for overnight before imaging on HRTEM. In Fig. 7, the pictograph distinctly reveals the blending of FSWCNTs onto the membrane eventually leading to the homogeneous distribution of uniform pores throughout the membrane. The chiral moiety gets homogeneously distributed in the membrane matrix. The circular patches in the micrograph indicate the pores or cavities of the membrane. It was observed that the membrane containing 0.2% of FSWCNTs consists of uniformly apportioned pores in comparison to the other membranes M_1, M_2 and M_3 that contained lower concentration of FSWCNTs which thereby verified the fact that the membrane pores got enhanced due to the addition of FSWCNTs.

The zeta potential of the membranes-pure polymeric membrane (PSf), M_1, M_2, M_3 and M_4 were determined from the values of streaming potential and streaming current obtained from the Electrokinetic analyzer. Fig. 8 depicts the plot of zeta potential values versus pH for all the prepared membranes. A membrane possessing antifouling characteristics tends to be quite efficient and this is determined by the zeta potential. The zeta potential of a membrane can be significantly increased by higher addition of FSWCNTs to the polymeric solution. The membrane containing greater amount of FSWCNTs had a more negative value of zeta potential due to the increment in the number of functional groups on the membrane surface. The pure polymeric membrane showed less negative zeta potential than the membranes containing FSWCNTs.

The contact angle for each of the membranes was evaluated using the sessile drop method which gave an insight about the membrane surface energy properties. The contact angle of the polysulfone and FSWCNTs based nanocomposite membranes are given in Fig. 9 as well as in Table 1. Carbon nanotubes are generally hydrophobic in nature [26]. However, after functionalization they become hydrophilic and as a result with increasing amount of FSWCNTs, the membrane hydrophilicity increases. Thus, concentration of FSWCNTs performs a crucial role in aggravating the hydrophilicity of the membrane which thereby increases the efficiency of the membrane in terms of chiral separation of racemic mixture. FSWCNTs particles found to have higher affinity to water than the neat polymeric membrane and hence hydrophilicity increases with increase in FSWCNTs in the neat membrane. Increase in membrane hydrophilicity could decrease the fouling behavior of the membrane [27]. At very high concentration of FSWCNTs, pore clogging occurs because of the aggregation of FSWCNTs in the membrane surface.

Tensile properties are important factors in order to determine the effective lifetime and strength of the membranes. Hence the mechanic performances of FSWCNTs based nanocomposite membranes were

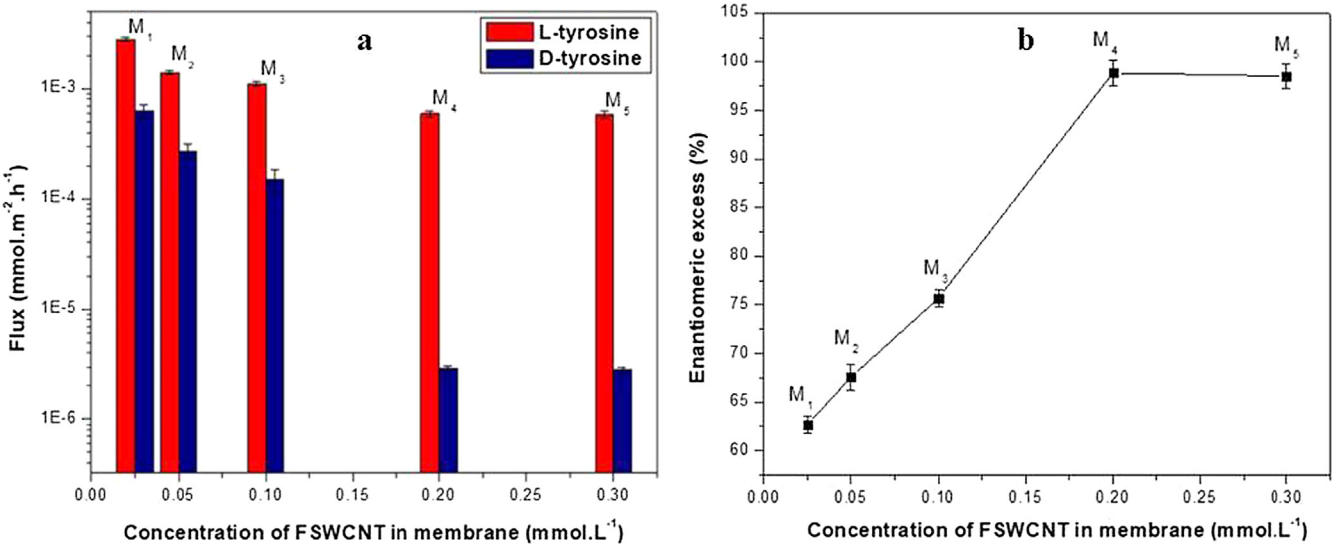

Fig. 10. Effect of FSWCNTs concentration in membranes for separation of D- and L-tyrosine after 8 h (a) Effect on flux (b) Effect on Enantiomeric excess, concentration of feed solution: 0.1 mmol·L^{-1}, flow rate: 25 mL·min^{-1}, transmembrane pressure: 4 bar, temperature: 35 °C.

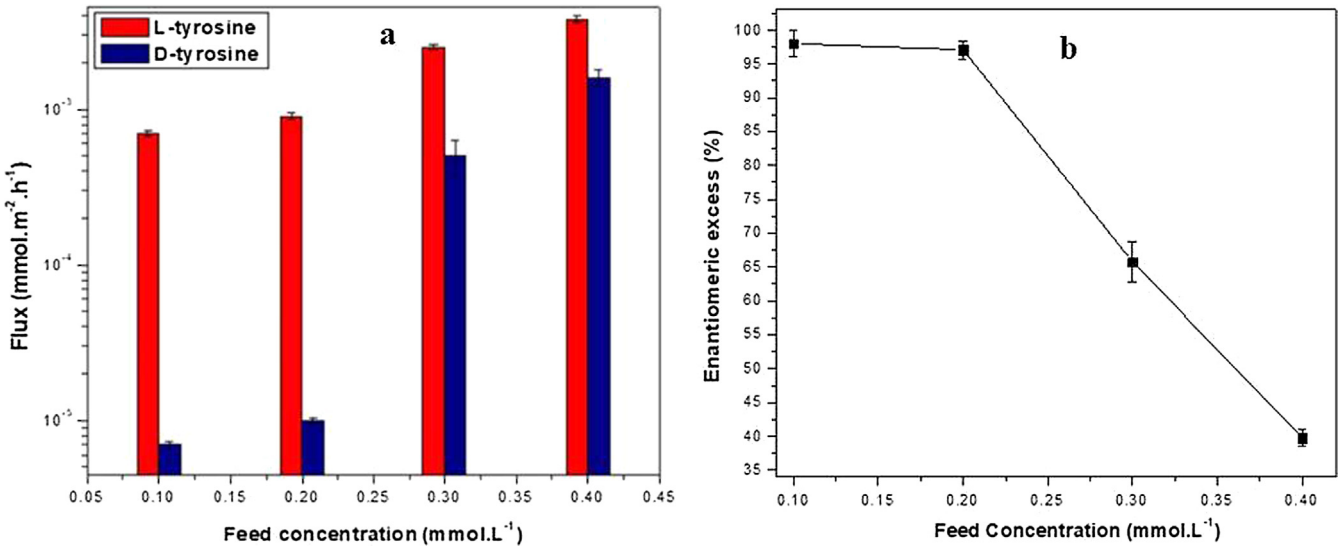

Fig. 11. Effect of feed concentration on separation of D- and L-tyrosine using M_4 membrane after 8 h (a) Effect on flux (b) Effect on Enantiomeric excess, flow rate: 25 mL·min^{-1}, transmembrane pressure: 4 bar, temperature: 35 °C.

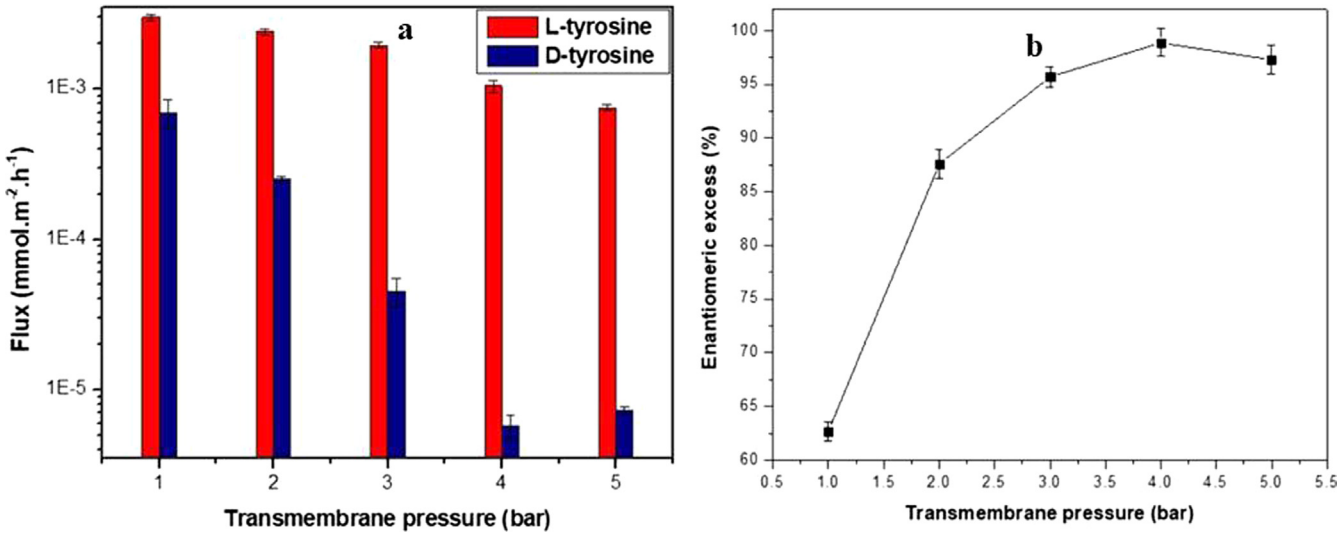

Fig. 12. Effect of pressure on separation of D- and L-tyrosine using M_4 membrane after 8 h (a) Effect on flux (b) Effect on Enantiomeric excess, concentration of feed solution: 0.1 mmol·L^{-1}, flow rate: 25 mL·min^{-1}, temperature: 35 °C.

determined by a UTM. The maximum tensile load of the membrane is 32 ± 0.4 N. The tensile strength of 0.2% of FSWCNTs containing membrane is the highest being 29 ± 0.4 MPa. Apparently, it was ascertained that the elongation break of the membrane containing higher concentration of FSWCNTs is also the highest. Thus, these properties are very much effective for performance of the membrane. Table 1 illustrates the values of the strength of the prepared membranes. It was observed that the strength was enhanced by the adding FSWCNTs in casting solution [28], however it is up to a certain level.

3.2. Results of separation study

The successive experiments were performed to evaluate the separation behavior of FSWCNTs based nanocomposite membranes. From the UHPLC data it is seen that the membrane selectively transports L-tyrosine relative to D-tyrosine, due to the selective binding of the chiral moiety to the D-isomer [11,29,30]. The change in the flux values for both L- and D- isomer were expressed in logarithmic form as it was the appropriate scale to depict the rate of change of the flux value over time. Apparently, the linear scale shows the absolute flux value over time which would not be appropriate to use in our work. Hence the logarithmic scale was used.

The concentration of the FSWCNTs is a pivotal criterion for enhancing the membrane pursuance in terms of the chiral resolution ability. Fig. 10(a and b) shows the effects of the concentration of FSWCNTs on flux and enantiomeric excess (ee) for a time period of 8 h. There is an upsurge in flux and enantiomeric excess value with the addition of higher amount of FSWCNTs in membrane. When the concentration of the FSWCNTs is 0.2% in casting solution (i.e. M_4 membrane), the permeation flux reaches up to 3×10^{-6} mmol·m^{-2}·h^{-1} and 5.9×10^{-4} mmol·m^{-2}·h^{-1} for D- and L-isomer respectively. It is also observed that there is sharp increment in ee values with the increase in the concentration of FSWCNTs. For the membrane containing 0.2% of FSWCNTs (M_4), the flux value of L-tyrosine is greater than D-tyrosine and in this case ee value was found to be 98.86%. Due to the increment in the surface area of functionalized SWCNTs, the self-association behavior of the membrane increases and as a result enantiomeric excess also increase [29,30]. Moreover, another set of experiment was also carried out using a membrane containing 0.3% of FSWCNTs and the flux value for this experiment remains almost similar. The ee value

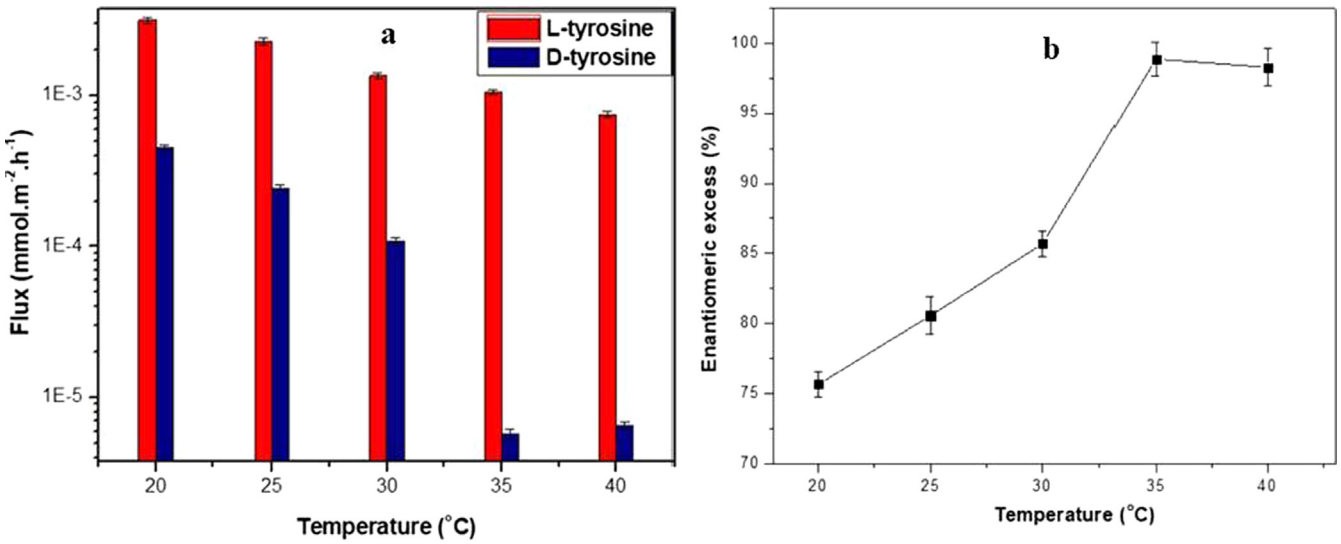

Fig. 13. Effect of temperature on separation of D- and L-tyrosine using M_4 membrane after 8 h (a) Effect on flux (b) Effect on Enantiomeric excess, concentration of feed solution: 0.1 mmol·L^{-1}, flow rate: 25 mL·min^{-1}, transmembrane pressure: 4 bar.

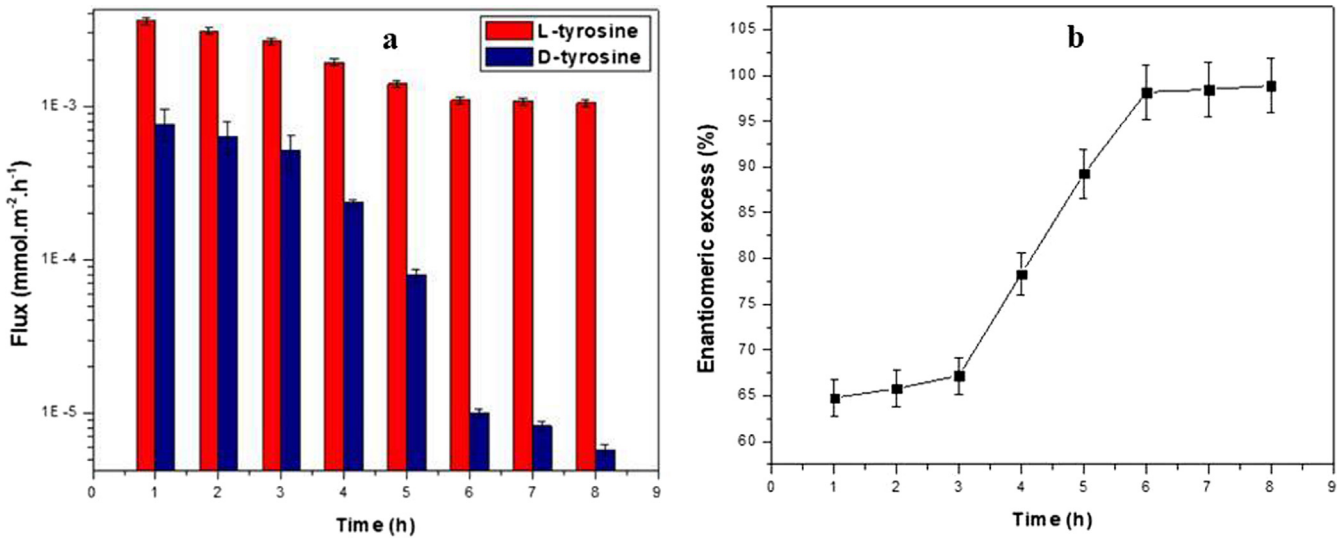

Fig. 14. Effect of time on separation of D- and L-tyrosine using M_4 membrane (a) Effect on flux (b) Effect on Enantiomeric excess, concentration of feed solution: 0.1 mmol·L^{-1}, flow rate: 25 mL·min^{-1}, transmembrane pressure: 4 bar, temperature: 35 °C.

Table 2
Results of UHPLC chromatograms.

Compound	Initial sample (feed solution)			Membrane treated sample (permeate solution)		
	Peak area (%)	Retention time, R_t (min)	Enantiomeric excess (%)	Peak area (%)	Retention time, R_t (min)	Enantiomeric excess (%)
D-Tyrosine	45.58	1.66	8.28	0.56	1.66	98.86
L-Tyrosine	53.84	2.25		98.06	2.25	

slightly decreases to 98.52% when compared to the one obtained in case of the M_4 membrane containing 0.2% of FSWCNTs. Based on this result, the further permeation experiments were conducted using the M_4 membrane only.

The impact of concentration of the feed solution on separation behavior of M_4 membrane is shown in Fig. 11(a and b) for a time period of 8 h. At a lower feed concentration of 0.1 mmol·L^{-1}, the ee % value is about 98%. Further, upon increasing the feed concentration gradually leads to the saturation of chiral moiety on the membrane surface for which there is limited interaction between the chiral moieties and the D-isomers as a result of which the flux value of D-tyrosine gradually increases and it eventually pass through the membrane. For the L-isomer, the change in flux value is almost consistent throughout as it gets permeated anyway. Apparently, this leads to a significant decrease in the ee value [29,30].

The impact of transmembrane pressure on M_4 membrane flux and ee % was studied as pressure is seemingly a propulsive parameter for evaluating membrane performance. The flux values for both D- and L-tyrosine first increases sharply and then slight increment is observed upon further increase in the pressure as seen in Fig. 12(a and b). Besides, the ee% value is approximately 98% at a pressure 4 bar. Further increment in the pressure that is above 4 bar, it was observed that there

is a decrement in the ee value due to the covenant effect amidst selectivity and permeation flux [28,31].

Another important factor that contributes to the membrane performance is the concentration polarization. Under the impact of optimum pressure and flow rate, tyrosine diffuses from the feed solution. As a result of which, there occurs deposition of tyrosine isomer on the membrane surface, which is because of the self-linkage of isomer and chiral moiety present in the membrane. When the solute concentration on the surface is somewhat higher than that in the core solution, there occurs a reversion in dissipation of tyrosine from the surface to the core solution. Apparently, there comes a point when this diffusion rate is equal to the dissipated movement of solute from the core phase to the surface of the membrane which leads to the formation of the boundary layer of concentration polarization [28].

The solubility, diffusion and mass transfer of solute in the core solution, viscosity of the core solution etc. are affected by the change in the temperature. As depicted in the Fig. 13(a and b), there is an increment in the value of ee with rise in the temperature varying from 20 °C to 35 °C. The fluxes of Tyrosine decrease with the decrease in the operating temperature which apparently raises the concentration of Tyrosine on the surface of the M_4 membrane. This leads to the increase in the formation of concentration polarization which reduces the enantioseparation ability of the FSWCNTs incorporated nanocomposite membrane. It is also observed that a significant higher temperature increases the diffusion rates from the feed solution and membrane which helps in eradicating the boundary layer of concentration polarization. Thus, a high value of ee was observed when the permeation experiment was done above a temperature of 25 °C. Another set of experiment was also conducted at 40 °C which revealed that upon further increasing the temperature, the flux value for D-isomer started increasing which apparently led to decrease in the ee value as depicted in Fig. 13(b). The reason behind this decrement might be due to the higher rate of diffusion of the feed solution through the membrane as a result of which the D-isomer doesn't get the optimum time to interact with the chiral moiety.

The impact of permeation time on separation behavior of M_4 membrane is shown in Fig. 14(a and b). Initially, the flux values tend to increase for both the isomers with the permeation time and finally after 7 h it reaches a saturation point. When the permeation experiment is carried for 1 h, the ee% value is about 64.76% which increases gradually till the permeation period reaches up to 7 h. Further, upon increasing the permeation time, there is no significant change in the ee value. The consistency in the ee value was perhaps due to the saturation of chiral moiety in the membrane for which there is limited interaction between the chiral moieties and the D-isomers for their self-association behavior [30].

Typical HPLC chromatograms of L-tyrosine (Standard), DL-tyrosine before and after 8 h of membrane treatment are given in the supporting information (Fig. S7). In order to identify the peaks for D- and L-isomers, a standard D-Tyrosine sample was analyzed along with the samples collected before and after membrane permeation experiment. The retention time and relative peak area for the standard, initial and the membrane treated samples are given in Table 2. It was evident from the chromatograms that upon 8 h of membrane treatment there was decline in the concentration of D-isomer with respect to the L-isomer from the racemic mixture as a result of the preferential permeability of L-isomer and self-linkage of D-isomer with the chiral moieties on the membrane surface.

4. Conclusions

SWCNT was functionalized successfully and confirmed by IR, Raman, XPS and FESEM analysis. To increase the hydrophilicity of the membrane, FSWCNT was used for preparation of chiral membrane for separation of DL-Tyrosine. The membrane was stable up to a temperature of 550 °C. The membrane surface roughness and mechanical strength were remarkably enhanced by the addition of FSWCNTs which in addition increases the permeation flux of the membrane for L-isomer. Higher enantiomeric excess upto 98.86% was obtained under optimized conditions which include the concentration of FSWCNTs as 0.2% in the membrane, operation pressure of 4 bar, feed concentration less than 0.1 $mmol{\cdot}L^{-1}$ and temperature of 35 °C. Slightly increase in temperature of the feed solution is favorable for removing the boundary layer formed during separation due to the concentration polarization in order to obtain a higher enantiomeric excess 98.86%. It is evident that the chiral separation of FSWCNTs based nanocomposite membrane is one of the most efficient membranes which have the possible potential to reduce the limitations in chiral separation using polymer-based membrane and may be replaced in place of other conventional processes for chiral separation.

Acknowledgement

Authors acknowledge CSIR New Delhi for financial support under HCP-0011 and Director, CSIR-NEIST for his keen interest on this work.

Appendix A. Supplementary material

Supplementary data to this article can be found online at https://doi.org/10.1016/j.seppur.2019.116061.

References

[1] J. Shen, Y. Okamoto, Efficient separation of enantiomers using stereoregular chiral polymers, Chem. Rev. 116 (2016) 1094–1138.
[2] M.F. Landoni, A. Soraci, Pharmacology of chiral compounds: 2-Arylpropionic acid derivatives, Curr. Drug Metab. 2 (2001) 37–51.
[3] N.M. Davies, X.V. Teng, Importance of chirality in drug therapy and pharmacy practice Implication for psychiatry, Adv. Pharm. 1 (2003) 242–252.
[4] A. Higuchi, M. Tamai, Y.A. Ko, Y.I. Tagawa, Y.H. Wu, B.D. Freeman, J.T. Bing, Y. Chang, Q.D. Ling, Polymeric membranes for chiral separation of pharmaceuticals and chemicals, Polym. Rev. 50 (2010) 113–143.
[5] M.K. Campbell, S.O. Farrell, Biochemistry, eight ed., Cengage Learning, USA, 2013.
[6] C. Meng, Y. Sheng, Q. Chen, H. Tan, H. Liu, Exceptional chiral separation of amino acid modified graphene oxide membranes with high flux, J. Membr. Sci. 526 (2017) 25–31.
[7] M. Rezakazemi, M. Sadrzadeh, T. Matsuura, Thermally stable polymers for advanced high-performance gas separation membranes, Prog. Energy Combust. Sci. 66 (2018) 1–4.
[8] L. Ma, X. Dong, M. Chen, L. Zhu, C. Wang, F. Yang, Y. Dong, Fabrication, water treatment application of carbon nanotubes (CNTs)-based composite membranes: a review, Membranes (Basel) 7 (2017) 16.
[9] A.H. El-Sheikh, J.A. Sweileh, Recent applications of carbon nanotubes in solid phase extraction and preconcentration: a review, Jordan J. of Chem. 6 (2011) 1–16.
[10] K. Shiomi, M. Yoshikawa, Multi-stage chiral separation with electrospun chitin nanofiber membranes, Sep. Purif. Technol. 118 (2013) 300–304.
[11] S. Hazarika, Enantioselective permeation of racemic alcohol through polymeric membrane, J. Mem. Sci. 310 (2008) 174–183.
[12] P.G. Ingole, H.C. Bajaj, K. Singh, Membrane separation processes: optical resolution of lysine and asparagines amino acids, Desalination 343 (2014) 75–81.
[13] H. Mizushima, M. Yoshikawa, N.W. Li, G.P. Robertson, M.D. Guiver, Electrospun nanofiber membranes from polysulfones with chiral selector aimed for optical resolution, Eur. Polym. J. 48 (2012) 1717–1725.
[14] H.D. Wang, R. Xie, C.H. Niu, H. Song, M. Yang, S. Liu, L.Y. Chu, Chitosan porous membranes for the sorption resolution of amino acid enantiomers, Chem. Eng. Sci. 64 (2009) 1462–1473.
[15] K. Singh, P.G. Ingole, J. Chaudhari, H. Bhrambhatt, A. Bhattacharya, H.C. Bajaj, Resolution of racemic mixture of α-amino acid derivative through composite membrane, J. Membr. Sci. 378 (2011) 531–540.
[16] J. Tobis, L. Boch, Y. Thomann, J.C. Tiller, Amphilic polymer conetworks as chiral separation membranes, J. Membr. Sci. 372 (2011) 219–227.
[17] K. Singh, P.G. Ingole, H. Bhrambhatt, A. Bhattachayra, H.C. Bajaj, Preparation, characterization and performance evaluation of chiral selective composite membranes, Sep. Purif. Technol. 78 (2011) 138–146.
[18] N. Saifuddin, A.Z. Raziah, A.R. Junizah, Carbon nanotube: a review on structure and their interaction with proteins, J. Chem. (2013) 1–18.
[19] V. Rastogi, P. Yadav, S.S. Bhattacharya, A.K. Mishra, N. Verma, A. Verma, J.K. Pandit, Carbon nanotubes: an emerging drug carrier for targeting cancer cells, J. Drug Deliv. (2014) 1–23.
[20] J. Yu, D. Huang, K. Huang, Y. Hong, Preparation of hydroxypropyl-β-cyclodextrin cross-linked multi-walled carbon nanotubes and their application in enantioseparation of clenbuterol, Chin. J. Chem. 29 (2011) 893–897.
[21] X. Wei, T. Tanaka, T. Hirakawa, M. Tsuzuki, G. Wang, Y. Yomogida, A. Hirano,

H. Kataura, High-yield and high-throughput single-chirality enantiomer separation of single-wall carbon nanotubes, Carbon 132 (2018) 1–7.
[22] M.S. Ata, R. Poon, A.M. Syed, J. Milne, I. Zhitomirsky, New developments in non-covalent surface modification, dispersion and electrophoretic deposition of carbon nanotubes, Carbon 130 (2018) 584–598.
[23] E. Soleymani, H. Alinezhad, M.D. Ganji, M. Tajbakhsha, Enantioseparation performance of CNTs as chiral selectors for the separation of ibuprofen isomers: a dispersion corrected DFT study, J. Mater. Chem. B 5 (2017) 6920.
[24] R. Abjameh, O. Moradi, J. Amani, The study of synthesis and functionalized single-walled carbon nanotubes with amide group, Int. Nano Lett. 4 (2) (2014) 97.
[25] P. Gogoi, Z. Zhang, Z. Geng, W. Liu, W. Hu, Y. Deng, Novel low temperature, low energy and high efficiency pretreatment technology for large wood chips with a redox couple catalyst, ChemSusChem 11 (6) (2018) 1121–1131.
[26] A.L. Hemasa, N. Naumovski, W.A. Maher, A. Ghanem, Application of carbon nanotubes in chiral and achiral separations of pharmaceuticals, Biol. Chem. Nanomater. 7 (2017) 186.
[27] Z. Ding, X. Liu, Y. Liu, L. Zhang, Enhancing the compatibility, hydrophilicity and mechanical properties of polysulfone ultrafiltration membranes with lignocelluloses nanofibrils, Polymers 8 (2016) 349–367.
[28] Z. Zhou, L. He, Y. Mao, W. Chai, Z. Ren, Green preparation and selective permeation of d-Tryptophan imprinted composite membrane for racemic tryptophan, Chem. Eng. J. 310 (2017) 63–71.
[29] S. Hazarika, N.N. Dutta, P.G. Rao, A quantitative structure activity relationship study on permeation of amino acids in enantioselective membranes, Appl. Membr. Sci. Technol. 2 (2006) 13–29.
[30] P.E.M. Overdevest, Enantiomer separation by ultrafiltration of enantioselective micelles in multistage systems, ISBN 90-5808-274-1.
[31] N.G. Sahoo, S. Rana, J.W. Cho, L. Li, S.H. Chan, Polymer nanocomposites based on functionalized carbon nanotubes, Progr. Polym. Sci. 35 (2010) 837–867.